Journal of Materials Chemistry C

Accepted Manuscript

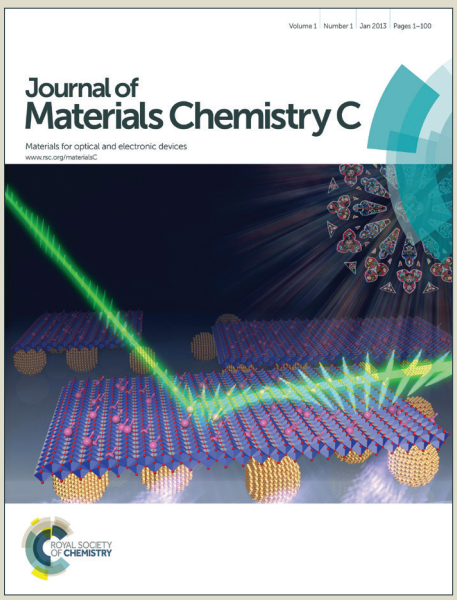

ROYAL SOCIETY OF CHEMISTRY

www.rsc.org/materialsC

Flexible $BaTiO_3$/PVDF gradated multilayer nanocomposite film with enhanced dielectric strength and high energy density

Received 00th January 20xx,
Accepted 00th January 20xx

DOI: 10.1039/x0xx00000x

www.rsc.org/

Y. N. Hao,[a] X. H. Wang,*[a] S. O'Brien,[b] J. Lombardi,[b] and L. T. Li[a]

Organic-inorganic 0-3 nanocomposites, which combine the potentially high dielectric strength of the organic matrix and the high dielectric permittivity of the inorganic filler, are extensively studied as energy-storage dielectrics in high-performance capacitors. In this study, a gradated multilayer $BaTiO_3$/poly(vinylidenefluoride) thin film structure is presented as a means to achieve both a higher breakdown strength and a superior energy-storage capability. The central layer of this film designed to provide the high electric displacement, is composed of high volume fraction 6-10 nm BTO nanocrystals produced by a TEG-sol method. The small particle size contributes to the high dispersibility of the nanocrystals in the polymer media, as well as a high interfacial area to mitigate the local electric field concentration. The outer layers of the structure are predominantly PVDF, with a significantly lower volume fraction of BTO, taking advantage of the higher dielectric strength for pure PVDF at the electrode-nanocomposite interface. The film is mechanically flexible, and can be removed from the substrate, with total thicknesses in the range of 1.2 – 1.5 μm. Parallel plate capacitance devices exhibit highly improved dielectric performances with low-frequency permittivity values of 20-25, a maximal discharged energy density of 19.37 J/cm^3 and dielectric (breakdown) strengths of up to 495 kV/mm.

Introduction

As a promising energy conversion and storage component, dielectric capacitors are cost-effective, environmentally friendly, and possess a distinctive high power density due to their very fast energy uptake and delivery. Thus, they could be used in numbers of modern electronics such as hybrid electric vehicles, medical devices and electrical weapon systems.[1] The energy storage capacity of dielectric capacitors highly relies on the dielectric layer and its internal structures. For this reason, high-performance dielectric materials and composites with enhanced energy density have been actively pursued for the past decade.[2]

In general, the energy density (U_e) of a dielectric material can be presented as

$$U_e = \int_{D_{max}}^{0} EdD \qquad (1)$$

Where E is the electric field and D is the electric displacement. Therefore, both high breakdown strength and large electric displacement are desired for a high energy density. Conventional dielectric materials are normally doped or modified ceramics with high dielectric constants, but in some cases temperature dependent breakdown strengths and loss characteristics occur that are undesirable. They are also discrete components with poor flexibility.[3] Polymer dielectric materials can sustain high electric fields, but they have too low permittivity values (ca. $\varepsilon_r < 10$) to meet the requirement for high U_e capacitors.[1,4] To avoid the drawbacks of these monolithic materials, great efforts have been made in preparing polymer-ceramic composites to obtain both the high breakdown strength and the superior dielectric properties.[5] However, high volume fraction of ceramic powders, usually >50 vol. %, are required for enhanced dielectric properties, which always lead to severe deterioration of the breakdown strength.[6] The significant reduction of the breakdown strength in the nanocomposites is attributed to the inhomogeneous local electric field concentration that is caused by the difference in permittivity between the polymer matrix and the ceramic filler.[7] Aggregation of the filler particles would further aggravate the local electric field concentration and reduce the capacitor device reliability.[8] Many methods have been used to solve these problems and enhance the breakdown strength of the $BaTiO_3$ based polymer nanocomposites, such as using surface-functionalized particles,[2,9] tailoring the interaction between $BaTiO_3$ nanoparticles and the polymer matrix,[10] using core-shell polymer@$BaTiO_3$ nanoparticles as filler,[11] and decorating the $BaTiO_3$ nanoparticles by ultra-small Ag nanoparticles.[12] While due to the limited variables and the filler properties, the energy density for the polymer-ceramic composite achieved so far is still too low to satisfy the industrial application.[2]

It was demonstrated that nanoscale filler particles, which can provide large interfacial areas, would promote the exchange coupling effect through a dipolar interface layer and afford higher polarization levels, dielectric response, and breakdown strength.[1,7,13] In this contribution, we report well-crystallized BTO nanoparticles with an average diameter of 8 nm applied in the gradated multilayer nanocomposite film. Many researchers observed the switching behaviour or the presence of local dipoles in such small BTO nanoparticles and suggested that large macroscopic polarization can be achieved in these nanocrystalline BTO particles.[14] Here, the 8-nm BTO nanoparticles with a high volume

[a] State Key Laboratory of New Ceramics and Fine Processing, School of Materials Science and Engineering, Tsinghua University, Beijing 100084, China. E-mail: wxh@mail.tsinghua.edu.cn; Tel: +86 10 62784579
[b] City University of New York, City College of New York, 13352 CDI, New York, NY 10031, USA

Electronic Supplementary Information (ESI) available: [details of any supplementary information available should be included here]. See DOI: 10.1039/x0xx00000x

fraction in the nanocomposite film can induce high electric displacement as well as mitigate the local electric field concentrations. Moreover, the small BTO nanoparticles are highly dispersed in the sol as well as the polymer matrix, which can easily solve the aggregation problem of the fillers. On the other hand, the macroscopic interface also plays an important role in the breakdown.[13,15] Wolak *et al.* imaged the dielectric breakdown behaviour of the multilayered polymer film and found that the layer boundaries can provide a path to deflect a breakdown to propagate laterally in the film, which was called "barrier effect".[16] Recently, Hu *et al.* expanded the traditional 0-3 nanocomposite to a multilayered topological-structure and realized both greater dielectric displacement and higher breakdown strength.[17] The multilayer structure design turns out to be an attractive way to further improve the energy density of the organic-inorganic nanocomposite. In addition, the development of thinner functional nanocomposite films is also an effective way to improve the breakdown.[15]

In this study, two kinds of functional layers, the outer polymer-rich layers and the internal BTO-rich layer, were introduced in the breakdown path of the BTO/PVDF nanocomposite film to achieve both the enhanced electrical displacement and high breakdown strength. The key to the process is the sequential deposition of uniform dispersions of the single component source, which generate a blended PVDF-BTO-PVDF structure prior to full evaporation of solvent and thermal treatment of the dielectric. In this process, the bottom polymer layer and the internal BTO layer were spin coated together to form a composite layer on the bottom electrode with 8-nm BTO nanoparticles distributed with a concentration gradient in the PVDF film, shown in figure 1. The bottom of this composite layer is PVDF with a small amount of BTO nanoparticles inside. It has a high breakdown strength that can substantially improve the overall breakdown strength of the multilayer nanocomposite film. The upper layer has a high volume fraction of 8-nm BTO nanoparticles. The small particles can afford a higher net polarization due to a larger interfacial area (compared to bigger particles), which can greatly enhance the electric displacement of the film. The pure PVDF layer was spin coated on this bottom nanocomposite film and formed the top high breakdown strength layer. The result is a 2-2 like sandwich structure with partial 0-3 character, seamless interfaces between layers and a concentration gradient of the BTO. Each of the functional layers is nanoscale and the total thickness of this nanocomposite film is 1.2 – 1.5 μm. By optimizing the fabrication conditions, flexible BTO/PVDF nanocomposite films with a maximal breakdown strength as high as 495 kV/mm and a discharged energy density of 19.37 J/cm^3 were obtained. This result confirms that multilayer structure design and finer BTO nanoparticles can further increase the energy density of the organic-inorganic nanocomposites and provides a new processing approach for developing nanocomposite films with high energy density.

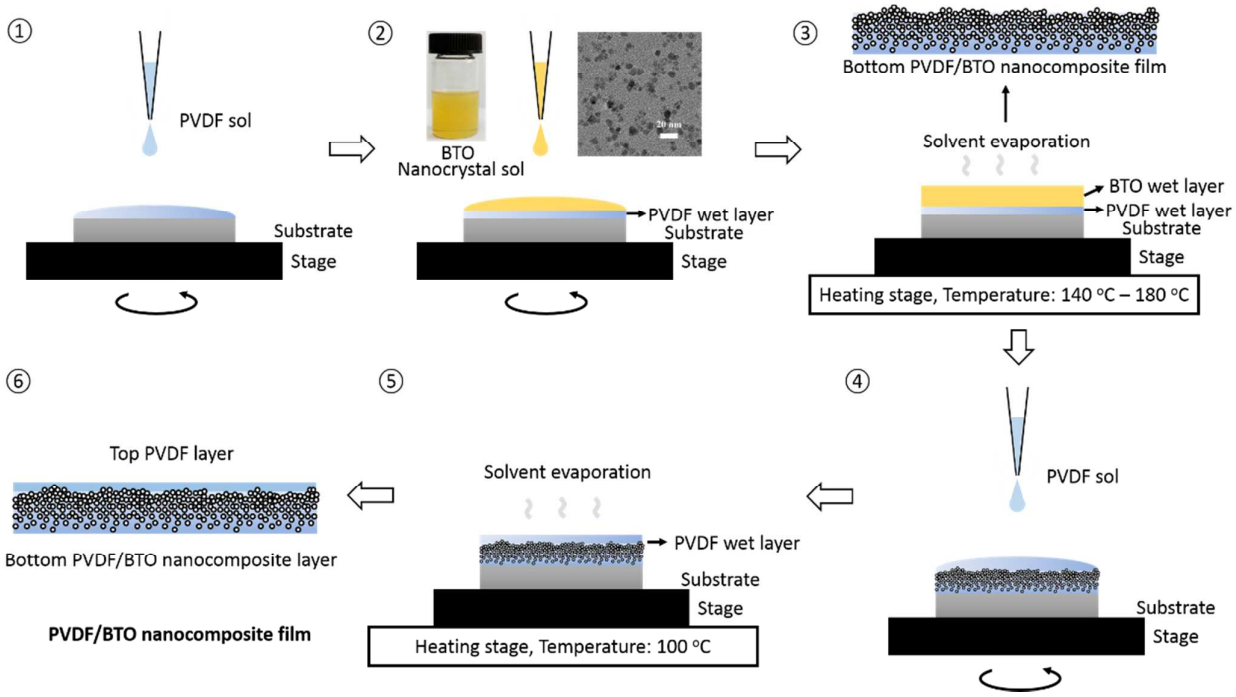

Fig. 1 Schematic diagram for the preparation of PVDF/BTO multilayer nanocomposite film.

Experimental

Materials and methods

The BTO nanocrystal sol was prepared by controlled hydrolysis of $Ti(OC_4H_9)_4$ in triethylene glycol (TEG), which has been reported earlier.[18] The highly stable semitransparent sol used in this study had a concentration of 0.8 mol/L and the average size of the BTO nanoparticles in it was about 8 nm. The PVDF sol was obtained by dissolving PVDF polymer in N,N-dimethylformamide (DMF) solvent at 60 °C and stirring for 30 minutes until the solution was transparent. The concentration of the PVDF sol was 0.1 g/mL. As shown in figure 1, to fabricate the BTO/PVDF nanocomposite film, a PVDF layer was firstly deposited on Pt-coated SiO_2/Si or Al substrate by spin coating of the PVDF sol at 5000 rpm for 30 s. Subsequently, a BTO nanoparticle layer was spin coated on the wet PVDF layer at 5000 rpm for 30 s using the nanocrystal sol. The as-prepared composite film was dried at 140 °C for 30 min and then 180 °C for 30 min for solvent evaporation. The thickness for this composite layer was about 900 nm. For the samples with different internal layers, one or three more BTO nanocrystal layers were deposited on the dried nanocomposite film and each layer has a thickness of ~ 50 nm. Finally, a top PVDF layer with a thickness of ~ 300 nm was spin coated on the composite film at the same condition. The sample with only the bottom nanocomposite layer and the top PVDF layer was marked as "P1BP", and the samples with additional one or three more BTO nanocrystal internal layers were marked as "P2BP" and "P4BP".

Characterizations

The transmission electron microscopy (TEM) image of the BTO nanoparticles was obtained by using a TEM (JEM-2010, JEOL Ltd., Tokyo, Japan) at an accelerating voltage of 200 kV. The surface and cross sectional morphology of the nanocomposite film and Energy Dispersive Spectrometer (EDS) line scanning spectrum were observed by a scanning electron microscope (SEM; JSM-7001F, JEOL Ltd., Tokyo, Japan) operated at 20 kV. The X-ray photoelectron spectroscopy (XPS; ESCALAB 250 Xi, Waltham, MA) was performed to study the BTO nanoparticle distribution in the bottom nanocomposite layer. The Fourier transform infrared spectroscopy (FT-IR) spectra were recorded on an FT-IR spectrometer (Vertex 70v, Bruker Ltd., Germany). X-ray diffraction (XRD) patterns of all samples were collected at room temperature by XRD (D/Max-2500; Rigaku Co., Tokyo, Japan) with CuKα radiation (λ = 1.5418 Å) operated at 40 kV and 200 mA. For dielectric measurements, gold electrodes of 3-mm diameter were evaporated on the surface of the nanocomposite films with an Al substrate. The dielectric permittivity and loss of the samples were measured using a precision impedance analyzer (4294A; Agilent, Palo Alto, CA). Thermogravimetric (TG) measurements and differential scanning calorimetry (DSC) curves of the sample were evaluated with a TG/DSC (STA 409PC, Netzsch, Selb, Germany). The ferroelectric hysteresis loop and the electric breakdown strength were measured by a ferroelectric test module (TF2000 analyzer; axi ACCT, Aachen, Germany) using the samples with sputtered 0.3-mm diameter platinum top electrodes on Pt-coated SiO_2/Si substrate.

Results and discussion

The yellow semitransparent BTO nanocrystal sol used in this method is shown in Figure 1. BTO nanoparticles with an average diameter as small as 8 nm were homogeneously dispersed in this sol from the inserted TEM observation. Recent research revealed that BTO nanoparticles do not follow the general prediction that the ferroelectric phase will vanish with smaller nanoparticles.[14] Instead, Li *et al.* has observed multiphase coexistence and a superior high Curie temperature for the 2.5 nm BTO nanoparticles by using aberration-corrected transmission electron microscopy under an in-situ heating holder.[19] Thus these 8-nm BTO nanoparticles are capable to show higher spontaneous polarizations and have the potential to provide enhanced electric displacement in the multilayer nanocomposite. As reported in our last paper,[18] this nanocrystal sol is highly stable, which can be easily utilized to fabricate BTO nanocrystal films with relatively high dielectric constant and large polarization. However, the existence of small interparticle void space deteriorated the voltage tolerance of the film and made it unsuitable for further investigation as an energy storage material. Here, by the multilayer structure design, we successfully obtained the gradated BTO-PVDF nanocomposite film with both the high breakdown strength and large electric displacement. During the solvent evaporation of the bottom PVDF-BTO nanocomposite layer, a rather low temperature of 140 °C was chosen to slow down the evaporation speed. The low temperature provides the two sols enough time to merge so that the BTO nanoparticles can gradually migrate into the PVDF polymer and finally form a gradient BTO distribution layer with high volume fraction of BTO on the upper layer and lower volume fraction on the bottom layer. Most importantly, this merging and diffusion process also lets PVDF fill the voids between the BTO nanoparticles and makes the nanocomposite a more dense, compact film, which can simultaneously make use of the high polarization of the BTO nanoparticles and improve the breakdown strength of the internal layer.

Although large amount of BTO nanoparticles were added into the multilayer nanocomposite, especially in the high concentration internal layer, the nanocomposite film can still possess high flexibility and transparency due to the small particle size. Figure 2 (a) shows the cross sectional SEM image of the uniform nanocomposite film with a thickness of 1.5 µm. Figure S1 shows a cross sectional SEM image of the film that was fractured in liquid nitrogen, from which the top PVDF layer and the bottom BTO/PVDF nanocomposite layer can be clearly observed. From Figure 2 (b), a rough interface between the bottom nanocomposite layer and the top layer can be observed through the transparent, slightly wrinkled surface PVDF layer. As this rough morphology was filled and covered by the top PVDF layer, finally they formed the multilayer nanocomposite film with a smooth surface. The rough interface between the surface PVDF layer and bottom nanocomposite layer can provide larger interface areas and stabilize the conjunction of the two layers. Figure 2 (c) is the photograph of the nanocomposite on a flexible aluminium foil substrate, which can be delaminated

from the substrate, (Figure 2d) showing its' continuous polymeric nature.

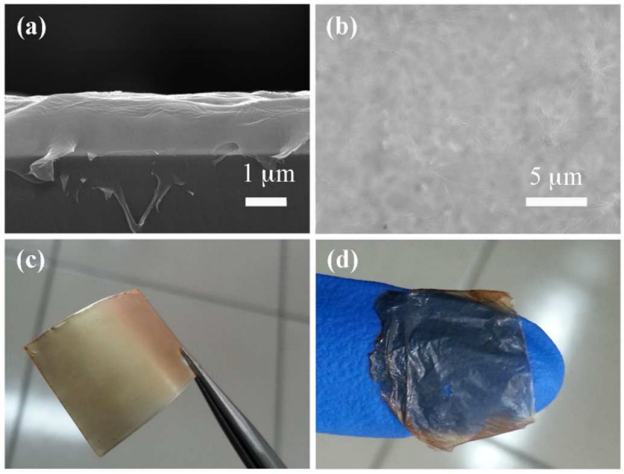

Fig. 2(a) Cross-sectional and (b) Surface SEM image of the BTO/PVDF nanocomposite film, showing a rough interface between the transparent top PVDF layer and the bottom nanocomposite layer. (c) Photograph of the nanocomposite on a flexible aluminium foil substrate, and (d) delaminated from the substrate, showing its' continuous polymeric nature.

PVDF is a semi-crystalline polymer that can exist in four different crystalline forms depending on the preparation methods such as temperature, stretching, and annealing conditions.[20] Of which β-phase is the most attractive one because it has the highest dipolar moment per unit cell (8×10^{-30} C m) compared to the other phases.[4] It was found that the multilayer nanocomposite film consisted of α-phase, β-phase, and γ-phase PVDF. As shown in the FT-IR spectra in Figure 3, the obvious absorbance bands at 614 and 764 cm^{-1} are the bending and wagging vibration of CF_2 group and the rocking vibration in the PVDF chain respectively, which demonstrated that the raw PVDF powder is nearly non-polar α-phase PVDF. The absorbance band at 874 cm^{-1} was generated from the CH_2 rocking and CF_2 stretching, while the bands at 1179 and 1210 cm^{-1} were attributed to the CH_2 wagging and rocking.[21] After the spin coating and heating process, both the multilayer nanocomposite film and the pure PVDF film showed strong β-phase bands at 840, 874, 1179, 1210 cm^{-1}, which confirmed that the processing method can promote the generation of high-performance ferroelectric β-phase PVDF towards improved polarization.

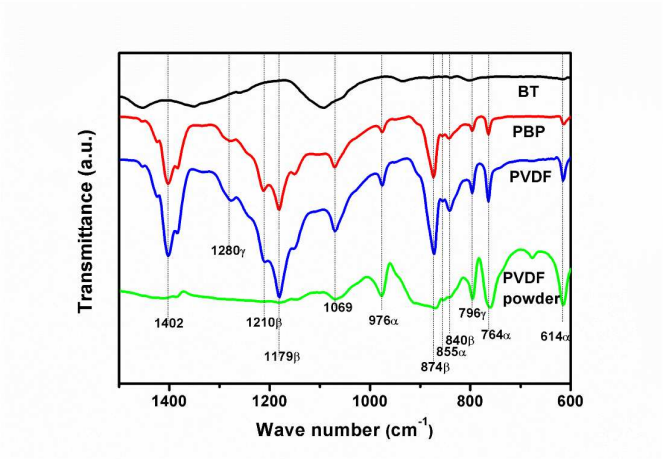

Fig. 3 FT-IR spectra of BTO nanocrystal film, sample P1BP, PVDF film and raw PVDF powder. Compared to the raw PVDF powder, PVDF film and the nanocomposite films show much stronger high-performance ferroelectric β-phase.

Phase structure of the pure PVDF film, the multilayer nanocomposite films and the BTO nanocrystal film were also detected by XRD, shown in Figure S2. The weak and broad peak at 2θ corresponding to 18° was assigned to α-PVDF and the peak at 2θ slightly higher than 20° was assigned to β-PVDF. In accordance with the FT-IR results, the multilayer nanocomposite films showed relatively high β-PVDF content. All the three samples showed intense BTO perovskite diffraction peaks and these peaks goes stronger with the increasing of the BTO nanocrystal layers. Because of the small particle size, the diffraction peaks for BTO were too broad to discriminate between the cubic and tetragonal phases.

The dielectric properties of the multilayer PVDF/BTO nanocomposite films and as a function of frequency at room temperature are presented in Figure 4. From Figure S3, it is observed that pure PVDF has a dielectric constant lower than 10. The high dielectric loss for the pure PVDF film at the low frequency end is induced by the permeation of the Pt electrode due to the high sputtering temperature and the low thickness of the film. And the dielectric loss at the high frequency end is caused by the glass transition of pure PVDF and the contact quality of the electrode. The dielectric constant for BTO nanocrystal film reaches 47 at low frequency (Figure S4) and shows very low dielectric loss. Due to the synthetic process, the nanoparticles have a surface TEG layer that measured as 10 wt. %, which makes it soluble in the polar solvent and disperses well in the polymer matrix. As this organic layer possesses a relatively high volume fraction which will partially fill the void space of the nanocrystal filler, the volume fraction of air in this film was calculated to be as low as 7.5 vol. % according to the modified Kerner Model and thus high dielectric values can be obtained. The modified Kerner Model[22] was used to predict the effective dielectric constant ε_{eff} for 0-3 type composite of nanocrystal fillers distributed in a continuous dielectric polymer host matrix. It takes account of dipolar interactions between pairs

of neighbouring spherical filler particles and leads to a modified local field in the medium,[22] which can be expressed as:

$$\varepsilon_{eff}=\frac{\varepsilon_h\cdot v_h+\varepsilon_f\cdot v_f\cdot(A)(B)}{v_h+v_f\cdot(A)(B)},$$

Where $A=\frac{3\varepsilon_h}{\varepsilon_f+2\varepsilon_h}$, and $B=1+\frac{3v_f\cdot(\varepsilon_f-\varepsilon_h)}{\varepsilon_f+2\varepsilon_h}$, (Eqn. 1)

Where ε_h, v_h and ε_f, v_f are the dielectric constants and volume fractions of the host and filler, respectively. Using this model, the total particle loading for P1BP, P2BP and P4BP was calculated to be 28, 32 and 37 vol. % according to the experimental value in Figure 4, which coincides well with the value that was calculated from the layer thickness. From this figure, the multilayer nanocomposite films have a dielectric constant approximately twice that of the pure PVDF film. It can be concluded that when more BTO nanocrystal layers are introduced, higher dielectric constants are obtained, as expected. The dielectric constant of the composite film slightly decreased with the increase of frequency. Compared to the pure PVDF film, the nanocomposite films showed higher heat resistance and presented lower and much more stable dielectric losses. The loss remains quite low (tan δ < 0.05) in the frequency range from 1-100 kHz. Due to the small nanoparticle filler, the nanocomposite film has large PVDF/nanoparticle interfaces, on which there may exist some ionizable hydroxyl groups.[6,23] Under the external electric field, these ionizable groups can migrate and aggregate at the interface, which would lead to interfacial polarization in the film. The high dielectric loss in the low frequency range from 40-100 Hz can be attributed to the space charge and interfacial polarization effects that are caused by the mobility of the ionizable hydroxyl groups on the interface. The linear increase of the dielectric loss at 0.1-10 MHz is attributed to the quality of contacts between the Pt electrodes and dielectric nanocomposite. Except that, there is also a glass transition relaxation peak of the PVDF polymer matrix at 0.1-10 MHz, which is denoted as α_a relaxation and couldn't be recognized due to the linear increase. Compared to the pure PVDF film, the dielectric loss at 0.1-10 MHz is significantly lowered, showing that α_a relaxation peak of PVDF is greatly restrained.

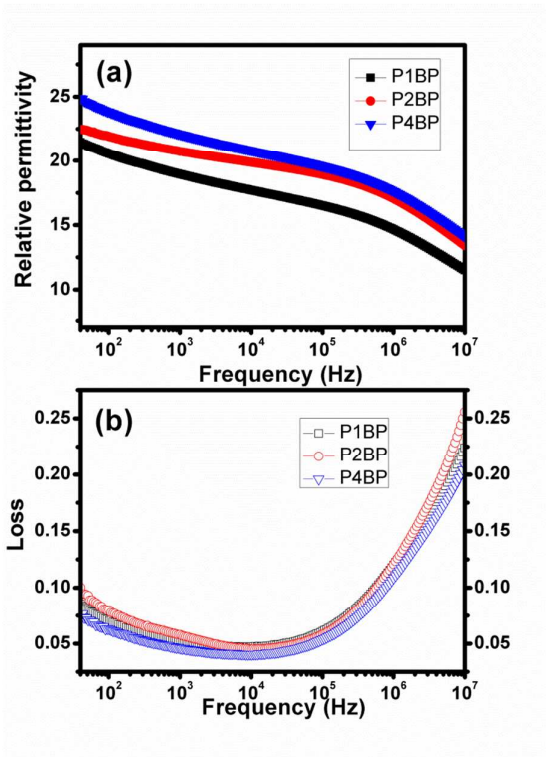

Fig. 4 Frequency-dependent (a) relative permittivity and (b) dielectric loss of parallel plate capacitance devices using samples P1BP, P2BP and P4BP as energy-storage layer. These parallel plate capacitance devices exhibit highly improved dielectric performances with low-frequency permittivity values of 20-25.

As shown from the processing method, the nanocomposite film is assumed to have a multilayer structure with a bottom layer composed of gradient BTO fraction in PVDF matrix and a pure PVDF top layer. As shown in the EDS line scanning analysis in figure S1, the Ba and Ti spectra show that BTO nanoparticles mainly distributed in the bottom nanocomposite layer and have a peak value at the internal layer, confirming the gradation of BTO nanoparticles. Correspondingly, C and F spectra show peak values at the outer layers, which certify the PVDF-rich outer layers. To further confirm the BTO nanoparticle loading and distribution in the PVDF polymer host matrix, XPS analysis was conducted on the two surfaces of the bottom nanocomposite layer, marked as point 1 and 2 on the inserted cross sectional SEM image for the nanocomposite film without a top PVDF layer, shown in Figure 5. According to the XPS analysis, the upper layer of the bottom nanocomposite layer has a relatively high BTO volume fraction of ~ 45 vol. % and the bottom layer has a BTO loading of ~ 18 vol. %, showing a gradient reduction from the top to the bottom, as illustrated in the inserted schematic diagram. Given that XPS is only a semiquantitative analysis, the BTO fraction might have an error of ± 15 wt%, which may cause big difference in the calculation of the dielectric constant. Therefore, we use the volume fraction value calculated from the experimental data to correct the XPS data, and by assuming that the BTO nanoparticles are linearly distributed in the

PVDF matrix from the surface to the bottom, the dielectric constant distribution in the whole layer was also calculated by the modified Kerner Model. As shown in Figure 6, the outer layers of this nanocomposite are PVDF-rich layers which can provide high breakdown strength and the internal layer is a BTO-rich layer with high electric displacement. TG/DSC analyses were also conducted on the "PBP" sample that was removed from the substrate, shown in Figure S5. From the TG curve, the volume fraction of BTO in "PBP" sample can be calculated to 28.9 vol%, which corresponds well with the volume fraction of ~ 28 vol% that was calculated from the dielectric constant. Owing to this structure, the breakdown strength of the nanocomposite film was significantly improved and the 8-nm BTO nanoparticles can then be polarized up to higher electric fields.

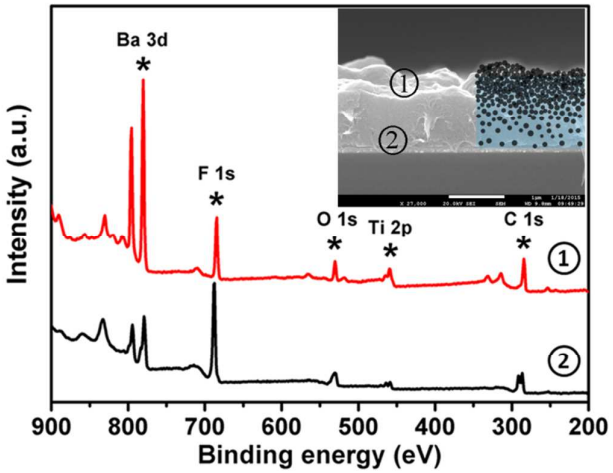

Fig. 5 XPS spectra of the two surfaces of the bottom nanocomposite layer, the inserted one is a SEM image of the bottom nanocomposite layer with a schematic diagram of the BTO distribution. The analyses show that the bottom nanocomposite layer is made up by gradiently distributed BTO nanoparticles in PVDF.

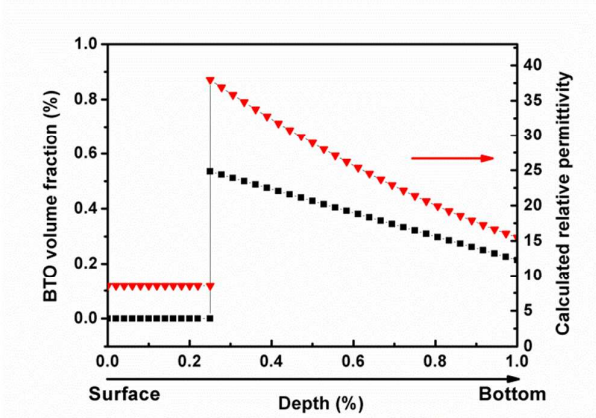

Figure 6. Assuming that the BTO nanoparticles are linearly distributed in the PVDF matrix from the surface to the bottom, dielectric constant distribution in the multilayer nanocomposite was calculated by a modified Kerner Model at 1 kHz. Permittivity values used were 84 for the 8-nm BTO nanoparticles and 8.5 for the polymer host matrix according to the experiment values. It shows that the outer layers of this nanocomposite are PVDF-rich layers which can provide high breakdown strength and the internal layer is a BTO-rich layer with high electric displacement.

The pure PVDF film fabricated under the same conditions has a breakdown strength of ~330kV/mm. Due to the high β-phase contents, it has an energy density of 6.9 J/cm^3. Although the pure BTO nanocrystal film possesses a very high electric displacement, the interspaces between the particles severely deteriorate the breakdown strength and lead to a rather low energy density value. After packing these two materials to the PVDF-BTO multilayer nanocomposite film, the breakdown strength for P1BP (*est*. 28% vol. BTO) was significantly improved to 495 kV/mm, which is 50% higher than that of the pure PVDF film. While for P2BP (*est*. 32% vol. BTO) and P4BP (*est.* 37% vol. BTO), the breakdown strengths were lowered to 428 and 385 kV/mm due to the reduced interparticle void space in the internal BTO nanocrystal layer. From Figure S6, the electric displacements of the nanocomposite films were also remarkably improved. The nanocomposite film P1BP exhibited a maximal electric displacement of 13.8 μC/cm^2. For the sample P4BP, the electric displacement was even increased to 16.7 μC/cm^2. As known, the influence of such small BTO nanoparticle fillers has not been investigated yet. According to Li *et al.*, surface relaxation is the origin of the coexistence of various phases in BTO particles under 10 nm. And the surface asymmetric phases significantly increased as the particle size decreased.[19] Recently, Zhu *et al.* reported that the BTO nanoparticles within 20 nm had increased c/a ratio along with the decreasing of the particle size.[14] In the films presented here, the high electric displacement value in the nanocomposite films were mainly induced by the polarization of the 8-nm BTO nanoparticles in the high nanoparticle concentration layer. Compared to the commercially available BTO powders, the 8-nm TEG synthesized BTO naonoparticles have the potential to provide higher electric displacements due to the increase in surface area and the increased ability to disperse them well into the PVDF matrix, which can enable higher volume fractions and reasonable interfacial contact and compatibility between the inorganic and organic components. Therefore the nanocomposite film can sustain higher electric fields.

The enhanced breakdown strength in the multilayer nanocomposite films can be explained by several mechanisms. Recent research has showed that polymer structural relaxations and dipolar trap states are strongly influenced by the polymer/oxide interface.[24] Because the interfaces between ceramic nanoparticles and polymers created effective electron scatterers and trapping centers, which can reduce the breakdown probability.[15,25] In the nanocomposite film, the well-dispersed 8-nm BTO nanoparticles had a high specific surface area. It can provide larger polymer/oxide interfaces to effectively reduce the stress concentration, block the degradation tree growth and thus increase the long-term breakdown strength of the film. Furthermore, the multilayer structure design let the electric field redistribute among the different functional layers. Assuming that the breakdown fields

in the bottom nanocomposite layer (E_c) and the top PVDF layer (E_p) follow the model of capacitors in series, i.e., $E_p/E_c \propto \varepsilon_c/\varepsilon_p$. As the top PVDF layer has a much lower dielectric constant (ε_p) than the bottom nanocomposite layer (ε_c), and the bottom nanocomposite layer also has a gradually increasing dielectric constant value from the bottom to the upper layer, the outer layers thus withstand local breakdown fields much higher than the overall breakdown strength, for instance, ~495 kV/mm for P1BP. Therefore, incomplete breakdown channels were generated in the higher dielectric constant internal layer, which can liberate the electric energy accumulation and alleviate the dielectric stress, at last avoid the complete breakdown of the multilayer nanocomposite film.[26] Based on the enhanced breakdown strength and the high electric displacement, the multilayer nanocomposite film presents a high energy storage capacity. Figure 7 displays the discharged energy densities obtained from the *D-E* loops as a function of applied electric field amplitude. For P1BP, a maximal discharged energy density of 19.37 J/cm^3 was obtained at 495 kV/mm. even for P2BP and P4BP, the maximal U_{dis} were as high as 16.98 and 13.46 J/cm^3.

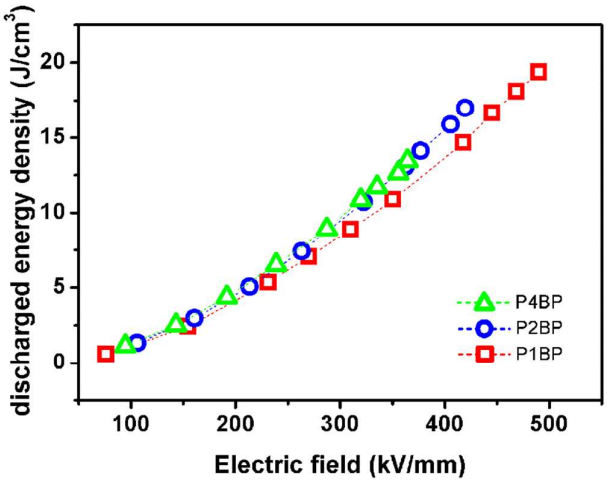

Fig. 7 Electric field-dependent discharged energy densities of samples P1BP, P2BP and P4BP.

Conclusions

In summary, gradated multilayer nanocomposite films with high flexibility and high dielectric and energy-storage properties were successfully fabricated using a sequential deposition spin coating method. A top layer of pure PVDF is combined with a 0-3 BTO-PVDF nanocomposite layer. The method allows for a gradated distribution of the BTO nanoparticles in the 0-3 layer, which due to their small size (~8 nm) are able to be well dispersed in the PVDF matrix and create a concentration gradient through the cross section of the film, estimated to be a 53% - 21% volume fraction in the BTO-PVDF layer. The nanocomposite films that consisted of a bottom gradient BTO distribution layer and a top pure PVDF layer can sustain high electric field with the outer layers and get high polarization with the internal layer. The increase in surface area of such small nanoparticle size, plus the increased ability to disperse them well into the PVDF matrix due to interfacial compatibility, enables higher volume fractions, more densely packed films, and a significantly reduced void volume fraction. This in turn leads to a higher electric field tolerance. The 8-nm BTO nanoparticles in the bottom nanocomposite layer can lower the local electric concentration through a larger interfacial area. As a result, the multilayer nanocomposite film with optimized gradient BTO distribution layer exhibited discharged energy density of 19.37 J/cm^3 with a dielectric strength of 495 kV/mm. The result revealed that this gradated multilayer structure design is an effective way in developing high energy density nanocomposites, and confirmed that smaller BTO nanoparticles can achieve higher volume fractions without deterioration of the breakdown strength of the film.

Acknowledgements

The acknowledgements come at the end of an article after the conclusions and before the notes and references.

Notes and references

1 Z.-M. Dang, J.-K. Yuan, S.-H. Yao, and R.-J. Liao, *Adv. Mater.,* 2013, **25**, 6334-65; B. Chu, X. Zhou, K. Ren, B. Neese, M. Lin, Q. Wang, F. Bauer, and Q. M. Zhang, *Science*, 2006, **313,** 334-6; A. Rabiee, H. Khorramdel, and J. Aghaei, *Renew. Sust. Energ. Rev.,* 2013, **18,** 316-26; X. Li, Y.-F. Lim, K. Yao, F. E. H. Tay, and K. H. Seah, *Phys. Chem. Chem. Phys.,* 2013, **15,** 515-20.

2 Y. Song, Y. Shen, P. Hu, Y. Lin, M. Li, and C. W. Nan, *Appl. Phys. Lett.,* 2012, **101,** 152904; L. Huang, S. Liu, B. J V. Tassell, X. Liu, A. Byro, H. Zhang, E. S Leland, D. L Akins, D. A Steingart, J. Li, and S. O'Brien, *Nanotechnology*, 2013, **24,** 415602; M. Rahimabady, K. Yao, S. Arabnejad, L. Lu, V. P. W. Shim, and D. Cheong Wun Chet, *Appl. Phys. Lett.,* 2012, **100**, 252907.

3 Z.-Y. Shen, W.-Q. Luo, Y.-M. Li, Q.-G. Hu, Z.-M. Wang, and X.-Y. Gu, *J. Mater. Sci.: Mater. El.,* 2012, **24,** 607-12; Z. Xie, B. Peng, S. Meng, Y. Zhou, Z. Yue, and S. E. Trolier-McKinstry, *J. Am. Ceram. Soc.,* 2013, **96,** 2061-64.

4 P. Martins, A. C. Lopes, and S. Lanceros-Mendez, *Prog. Polym. Sci.,* 2014, **39,** 683-706.

5 P. Kim, N. M. Doss, J. P. Tillotson, P. J. Hotchkiss, M.-J. Pan, S. R. Marder, J. Li, J. P. Calame, and J. W. Perry, *Acs Nano,* 2009, **3,** 2581-92; K. Yu, H. Wang, Y. Zhou, Y. Bai, and Y. Niu, *J. Appl. Phys.,* 2013, **113,** 034105.

6 B. Luo, X. Wang, Y. Wang, and L. Li, *J. Mater. Chem. A,* 2014, **2,** 510-19; Z.-M. Dang, Y.-Q. Lin, H.-P. Xu, C.-Y. Shi, S.-T. Li, and J. Bai, *Adv. Funct. Mater.,* 2008, **18,** 1509-17.

7 Y. U. Wang, and D. Q. Tan, *J. Appl. Phys.,* 2011, **109,** 104102; J. Y. Li, L. Zhang, and S. Ducharme, *Appl. Phys. Lett.,* 2007, **90,** 132901; P. Kim, S. C. Jones, P. J. Hotchkiss, J. N. Haddock, B. Kippelen, S. R. Marder, and J. W. Perry, *Adv. Mater.,* 2007, **19,** 1001-05; M. Arbatti, X. Shan, and Z. Y. Cheng, *Adv. Mater.,* 2007, **19,** 1369-72.

8 Y. Song, Y. Shen, H. Liu, Y. Lin, M. Li, and C.-W. Nan, *J. Mater. Chem.,* 2012, **22,** 8063; J. Li, J. Claude, L. E. Norena-Franco, S. I. Seok, and Q. Wang, *Chem. Mater.,* 2008, **20**, 6304-6.

9 M.-F. Lin, V. K. Thakur, E. J. Tan, and P. S. Lee, *RSC Adv.,* 2011, **1,** 576.

10 K. Yang, X. Huang, Y. Huang, L. Xie, and P. Jiang, *Chem. Mater.*, 2013, **25**, 2327-38.
11 M. Zhu, X. Huang, K. Yang, X. Zhai, J. Zhang, J. He, and P. Jiang, *ACS Appl. Mater. Interfaces*, 2014, **6**, 19644-54; X. Huang, and P. Jiang, *Adv. Mater.*, 2015, **27**, 546-54.
12 L. Xie, X. Huang, B. Li, C. Zhi, T. Tanaka, and P. Jiang, *Phys. Chem. Chem. Phys.*, 2013, **15**, 17560-9.
13 J. Li, *Phys. Rev. Lett.,* 2003, **90,** 217601; N. Guo, S. A. DiBenedetto, D.-K. Kwon, L. Wang, M. T. Russell, M. T. Lanagan, A. Facchetti, and T. J. Marks, *J. Am. Chem. Soc.,* 2007, **129,** 766-7; J. Li, S. I. Seok, B. Chu, F. Dogan, Q. Zhang, and Q. Wang, *Adv. Mater.,* 2009, **21**, 217-21; Z.-M. Dang, D. Xie, and C.-Y. Shi, *Appl. Phys. Lett.,* 2007, **91,** 222902.
14 F. A. Rabuffetti and R. L. Brutchey, *J. Am. Chem. Soc.,* 2012, **134,** 9475-87; N. Nuraje, K. Su, A. Haboosheh, J. Samson, E. P. Manning, N. l. Yang, and H. Matsui, *Adv. Mater.,* 2006, **18,** 807-11; V. Bansal, P. Poddar, A. Ahmad, and M. Sastry, *J. Am. Chem. Soc.,* 2006, **128,** 6; J. Zhu, W. Han, H. Zhang, Z. Yuan, X. Wang, L. Li, and C. Jin, *J. Appl. Phys.,* 2012, **112,** 064110.
15 R. Vogelsang, T. Farr, K. FrÃ¶hlich, *IEEE T. Dielect. El. In.,* 2006, **13,** 373-82; N. Guo, S. A. DiBenedetto, P. Tewari, M. T. Lanagan, M. A. Ratner, and T. J. Marks, *Chem. Mater.,* 2010, **22,** 1567-78; T. J. Lewis, *J. Phys. D: Appl. Phys.,* 2005, **38,** 202-12; D. P. Agoris, I. Vitellas, O. S. Gefle, S. M. Lebedev and Y. P. Pokholkov, *J. Phys. D: Appl. Phys.,* 2001, **34,** 3485.
16 M. A. Wolak, A. S. Wan, J. S. Shirk, M. Mackey, A. Hiltner, and E. Baer, *J. Appl. Polym. Sci.,* 2012, **123,** 2548-57.
17 P. Hu, Y. Shen, Y. Guan, X. Zhang, Y. Lin, Q. Zhang, and C.-W. Nan, *Adv. Funct. Mater.,* 2014, **24,** 3172-78.
18 Y. Hao, X. Wang, J. Kim, L. Li, and D. Lupascu, *J. Am. Ceram. Soc.,* 2014, **97,** 3434-41.
19 Y. Li, Z. Liao, F. Fang, X. Wang, L. Li, and J. Zhu, *Appl. Phys. Lett.,* 2014, **105,** 182901.
20 P. Thomas, *EXPRESS Polym. Lett.,* 2010, **4,** 632-43.
21 L. Yu and P. Cebe, *Polymer,* 2009, **50,** 2133-41.
22 P. Kim, N. M. Doss, J. P. Tillotson, P. J. Hotchkiss, M.-J. Pan, S. R. Marder, J. Li, J. P. Calame, and J. W. Perry, *ACS Nano*, 2009, **3,** 2581-92.
23 M.-F. Lin, V. K. Thakur, E. J. Tan and P. S. Lee, RSC Adv., 2011, 1, 576-8.
24 P. Tewari, R. Rajagopalan, E. Furman, and M. T. Lanagan, *J. Colloid Interf. Sci.,* 2009, **332,** 65-73.
25 T. Imai, F. Sawa, T. Nakano, T. Ozaki, T. Shimizu, M. Kozako, and T. Tanaka, *IEEE T. Dielect. El. In.,* 2006, **13,** 319-26; R. C. Smith, C. Liang, M. Landry, J. K. Nelson, and L. S. Schadler, *IEEE T. Dielect. El. In.,* 2008, **15,** 187-96; H. Uehara and K. Kudo, *IEEE T. Dielect. El. In.,* 2005, **12,** 1266-71.
26 L. A. Fredin, Z. Li, M. T. Lanagan, M. A. Ratner, and T. J. Marks, *Adv. Funct. Mater.,* 2013, **23,** 3560-69; D. P. Agoris, I. Vitellas, O. S. Gefle, S. M. Lebedev, and Y. P. Pokholkov, *J. Phys. D: Appl. Phys.,* 2001, **34,** 3485-91.

$BaTiO_3$/PVDF nanocomposite film with high flexibility and gradated $BaTiO_3$ distribution structure is fabricated by sequential deposition of uniform dispersions of pure PVDF and 8-nm $BaTiO_3$ nanoparticle sol. These films show high low-frequency dielectric constents of 20-25 with low dispation, a maximal discharged energy density values of 19.37 J/cm^3 and dielectric breakdown strengths of up to 495 kV/mm.

Keyword: PVDF, $BaTiO_3$, nanocomposite film, energy density, dielectric

Yanan Hao,[a] Xiaohui Wang,*[a] Stephen O'Brien,[b] Julien Lombardi,[b] and Longtu Li[a]

Flexible $BaTiO_3$/PVDF gradated multilayer nanocomposite film with enhanced dielectric strength and high energy density